Research Article Vol. 59, No. 3 / 20 January 2020 / Applied Optics 701

applied optics

# Structured light beams created through a multimode fiber via virtual Fourier filtering based on digital optical phase conjugation

Chaojie Ma,[1] Jianglei Di,[1] Jiazhen Dou,[1] Peng Li,[1] Fajun Xiao,[1] Kaihui Liu,[2] Xuedong Bai,[3] and Jianlin Zhao[1,*]

[1]MOE Key Laboratory of Material Physics and Chemistry under Extraordinary Conditions, and Shaanxi Key Laboratory of Optical Information Technology, School of Science, Northwestern Polytechnical University, Xi'an 710072, China
[2]State Key Laboratory for Mesoscopic Physics, School of Physics, Peking University, Beijing 100871, China
[3]Institute of Physics, Chinese Academy of Sciences, Beijing 100080, China
*Corresponding author: jlzhao@nwpu.edu.cn

Received 9 October 2019; revised 25 November 2019; accepted 9 December 2019; posted 9 December 2019 (Doc. ID 380058); published 15 January 2020

**Digital optical phase conjugation (DOPC) is a newly developed technique in wavefront shaping to control light propagation through complex media. Currently, DOPC has been demonstrated for the reconstruction of two- and three-dimensional targets and enabled important applications in many areas. Nevertheless, the reconstruction results are only phase conjugated to the original input targets. Herein, we demonstrate that DOPC could be further developed for creating structured light beams through a multimode fiber (MMF). By applying annular filtering in the virtual Fourier domain of the acquired speckle field, we realize the creation of the quasi-Bessel and donut beams through the MMF. In principle, arbitrary amplitude and/or phase circular symmetry filtering could be performed in the Fourier domain, thus generating the corresponding point spread functions. We expect that the reported technique can be useful for super-resolution endoscopic imaging and optical manipulation through MMFs.** 

https://doi.org/10.1364/AO.380058

## 1. INTRODUCTION

Optical fibers can guide light between separate locations as well as deliver and collect information, enabling their significant applications in telecommunication and biomedical fields [1,2]. Due to their flexible nature, optical fibers have been used for a new type of endoscope and are key optical elements for flexible endoscopic systems [2,3]. Compared with conventional optical microscopes, flexible endoscopes can provide minimally invasive images deep within tissues [2]. Traditional flexible endoscopes are usually constructed using a fiber bundle or a single-mode fiber with additional distal optical elements, which suffer from either a low spatial resolution or a large diameter [2–6]. Recently, multimode fibers (MMFs) with a large number of degrees of freedom and parallel information transport ability have attracted intense interest and are considered as ideal elements for ultra-thin endoscopic imaging [3,4]. However, coherent light propagation in a MMF experiences phase randomization due to modal scrambling, thereby generating speckle patterns [5]. The complex process makes a major obstacle for direct imaging and information transfer through MMFs but actually is deterministic. To overcome this challenge, different wavefront-shaping techniques, originally developed in research involving highly scattering media [7–15], are extended to MMFs, including transmission matrix measurement, iterative wavefront optimization, and digital optical phase conjugation (DOPC) [16–25]. Remarkable progress has been made in MMFs by using wavefront-shaping techniques, such as diffraction-limited focusing, fluorescence scanning imaging, and wide-field imaging [3–5]. In comparison, DOPC determines the optimum wavefront with a single-shot measurement and thus shows the shortest average response time per degree of freedom [26,27].

DOPC is based on the time-reversal principle to suppress multiple scattering effects of complex media. Unlike analog optical phase conjugation (OPC) based on nonlinear crystals, DOPC is achieved by using two devices, a digital image sensor and a spatial light modulator (SLM) [13,14]. Thus, DOPC shows several intrinsic advantages over analog OPC, such as the higher fluence reflectivity and flexibly adjustable phase conjugation wavefront [26]. The first demonstration of DOPC for the turbidity suppression of scattering medium was presented

by Cui and Yang [13]. Subsequently, DOPC was applied to biomedical tissues, MMFs, and multicore fibers [25–39]. And the reconstruction of two-dimensional wide-field images and three-dimensional structured light beams has been demonstrated by using DOPC [40,41]. Nevertheless, due to the time-reversal principle, the reconstruction results are phase conjugated to the original input targets. In other words, DOPC could only be used to regenerate the input target rather than generate a new one. Although the angular memory effect of traditional scattering media could be combined with DOPC to generate multiple focal spots, the result is just a simple duplication of the original reconstructed focus. In contrast to traditional scattering media, MMFs feature the cylindrical symmetry and show the rotational memory effect [17,42–44]. As a result, in MMFs there exist the propagation-invariant modes that maintain their transverse field distributions during light propagation [43,44]. By selecting the appropriate mode or incident angle coupled into the MMF, the quasi-Bessel and donut beams were generated through the fiber [45–47]. In addition, using the cylindrical symmetry feature, the measured transmission matrix technique has been developed to generate a quasi-Bessel beam through the MMF by adding an annular mask on the SLM plane [17]. Recently, the rotational memory effect of MMFs has been exploited for multiple-spot focusing based on DOPC [48]. However, the achievement of modulating the reconstructed target has not been verified based on DOPC.

In this paper, we report an approach specially applied to MMFs for the creation of structured light beams based on DOPC. To the best of our knowledge, this is the first time that the DOPC technique has been developed to create a focal spot with the intensity distribution different from the original input target. Here, taking advantage of the cylindrical symmetry of MMFs, we build a filtering operator in the virtual Fourier domain of the speckle field acquired based on DOPC. From this operator, we demonstrate the creation of the quasi-Bessel and donut beams by using simple annular filtering. The created quasi-Bessel beam shows a smaller focus size and a longer depth of focus in comparison with the regenerated Gaussian focus. In principle, arbitrary amplitude and/or phase circular symmetry masks could be applied, thus enabling the creation of the corresponding point spread functions.

## 2. EXPERIMENTAL SETUP

Figure 1 shows the schematic of the implementation system for the achievement of DOPC, which is on the basis of our previous experimental setup [41,48]. The laser source used is a diode-pumped solid-state laser with a wavelength of 532 nm. The laser beam is expanded and collimated via a microscope objective, $MO_1$, a pinhole, and a lens, $L_1$. The collimated beam passes through a half-wave plate (HWP) to adjust its polarization state and then is split into a sample beam and reference beam by a polarizing beam splitter (PBS). The sample beam is first magnified through a $4f$ system composed of the lenses $L_4$ and $L_5$. Subsequently, the magnified beam is focused by a microscope objective, $MO_2$ (Newport, M-20×, NA = 0.4) to form a Gaussian focus, which is used to be coupled into a commercial step-index MMF (YFOC, approximately 19 cm length, 105 μm core diameter, NA = 0.22). Due to modal scrambling, the speckle field is generated at the fiber output facet, which is imaged on the complementary metal-oxide-semiconductor (CMOS) (MotionBLITZ EoSens Cube7) target via a microscope objective, $MO_3$ (Newport, M-40×, NA = 0.65) and lens $L_6$. The reference beam is incident on a reflective phase-only SLM (Holoeye, Pluto-Vis). The SLM plane is directly imaged on the CMOS target through a $4f$ system composed of lenses $L_2$ and $L_3$, which could address the challenging alignments in DOPC [28,40,48]. Finally, the speckle field and reference beam interfere with each other on the CMOS target to form an off-axis hologram. To retrieve the phase information of the speckle field, we use a very effective and versatile numerical reconstruction technique, the angular spectrum method [49], with the need of twice fast Fourier transforms (FFTs). The retrieved phase information is displayed on the SLM to generate the phase-conjugate wavefront of the speckle field, which is delivered back to the MMF after being reflected by the mirror (M), positioned at the equivalent plane of the CMOS. Finally, a charge-coupled device (CCD) is used to record the phase-conjugate focus via an imaging system composed of the $MO_2$ and lens $L_7$.

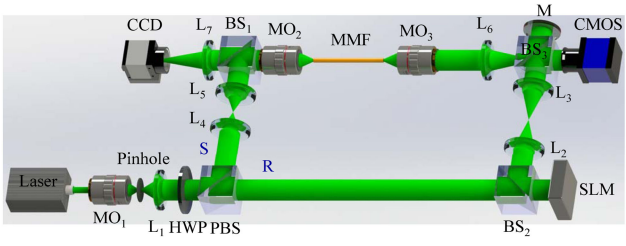


**Fig. 1.** Schematic of the implementation system for the achievement of DOPC. $MO_1 - MO_3$, microscope objectives; $L_1 - L_7$, lenses; HWP, half-wave plate; PBS, polarizing beam splitter; $BS_1 - BS_3$, beam splitters; M, mirror.

## 3. EXPERIMENTAL RESULTS

Figure 2 depicts the principle for realizing the creation of structured light beams through a MMF based on DOPC. First, as the formed Gaussian focus is coupled near the fiber core axis at the distance of approximately 100 μm in front of the fiber, the resulting off-axis hologram is recorded. Its spatial spectra can be obtained by taking a two-dimensional FFT. Then, extract and select one of the first orders containing the original scattered wave information with a bandpass filter (BF), marked with a

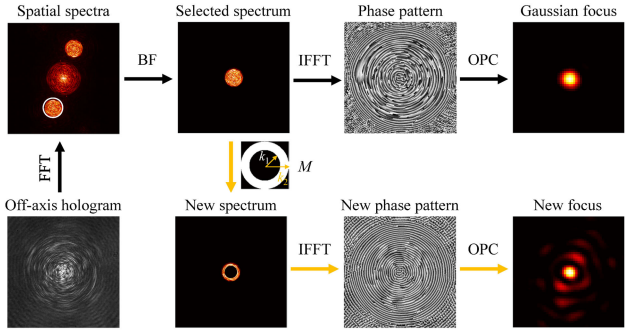


**Fig. 2.** Principle for the creation of structured light beams through a MMF based on DOPC.

white circle, and recenter it in the Fourier domain. In general, an inverse FFT (IFFT) is applied to the selected spectrum to acquire the phase information of a speckle field, which is digitally reversed and then linearly transformed into gray scale to display on the SLM. To accomplish OPC playback, the phase-conjugate wavefront must be precisely overlapped with the original scattered wavefront [48]. When the sample beam is blocked, a regenerated Gaussian focus is recorded using the CCD. Its peak-to-background ratio (PBR), defined as the ratio between the peak intensity of the focus and the mean intensity of a speckle field generated with a blank pattern displayed on the SLM, is evaluated to be approximately 1100.

Taking advantage of the cylindrical symmetry of MMFs [43,44], we build an operator by numerically applying a circular symmetry mask $M$ in the selected spectrum. The mask is first designed with the same size to the BF in the Fourier domain. Therefore, before being added in the Fourier domain, it is expanded by the zero padding to have the identical number of pixels to the recorded hologram. First, we design an amplitude annular mask $M$, which can be expressed by

$$M(k) = \begin{cases} 1, & k_1 \le k \le k_2 \\ 0, & \text{else} \end{cases}, \tag{1}$$

where $k$ is the radius of the pupil size in $k$ space. Here, the amplitude mask with the annular thickness 36% of the pupil size is applied in the Fourier domain and only the high-frequency information. From this, we could acquire a new spectrum and the corresponding new phase pattern. Similarly, the new acquired phase pattern is displayed on the SLM for accomplishing OPC playback, and a sharp focus is still presented on the CCD target. In the same experimental condition, its PBR is evaluated to be approximately 400.

To prove the creation of the structured light beam, the three-dimensional intensity profiles of two focal spots are characterized, as shown in Fig. 3, where Figs. 3(a) and 3(b) give the intensity profiles of two focal spots along the horizontal direction, respectively. The full width at half-maximum (FWHM) of the regenerated Gaussian focal spot is measured to be 1.28 μm, close to the diffraction limit for the used MMF calculated as $\lambda/(2\mathrm{NA}) \approx 1.21$ μm. The FWHM of the new generated focal spot is 1.09 μm, smaller than the Gaussian focus and diffraction limit. To characterize the beam propagation ($z$-axis) feature, a series of focal intensity images at the different positions along the $z$ axis are recorded using the CCD by scanning $MO_2$. Figures 3(c) and 3(d) show the calculated normalized intensity distributions in the $yz$ plane of two focal spots, respectively. Figure 3(e) presents the corresponding intensity profiles along the $z$ axis. It is shown that the created smaller focal spot has a longer depth of focus, which is about 1.9 times than that of the Gaussian focus. As is known to all, quasi-Bessel beams show the properties of smaller focus size and propagation invariant over a limited propagation distance, which have been used to improve imaging depth and resolution [50,51]. Therefore, we prove without ambiguity that a quasi-Bessel beam is created through the MMF by using virtual annular filtering. An amplitude mask with a narrower annular thickness would result in the focus with a smaller size and longer depth of focus, but with a lower PBR. Here, it should be mentioned that the used MMF actually features unperfect cylindrical symmetry, because of the uneven fiber facet and the fiber with a slight bending deformation [48]. Despite this, the generation of a quasi-Bessel beam through the MMF could be still achieved.

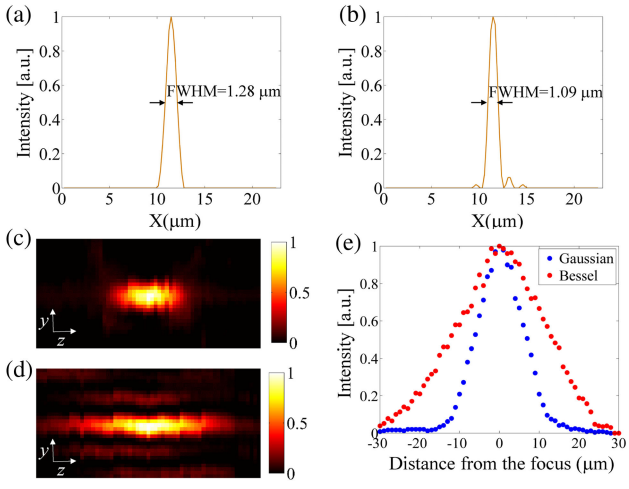


**Fig. 3.** Measurement results for three-dimensional profiles of the regenerated Gaussian and new created focal spots. (a) and (b) Intensity profiles of two focal spots along the horizontal direction, respectively; (c) and (d) calculated normalized intensity distributions in the $yz$ plane of two focal spots, respectively; (e) intensity profiles along the $z$ axis of (c) and (d).

Analogous to filtering performed in free space, an amplitude annular mask applied in the virtual Fourier domain of speckle field could be used to create a quasi-Bessel beam through the MMF. Moreover, the creation of the quasi-Bessel beam also shows the deterministic focusing by using the filtering operator. We then design a phase annular mask $M$, which can be expressed by

$$M(k) = \begin{cases} 1, & k_1 \le k \le k_2 \\ -1, & \text{else} \end{cases}. \tag{2}$$

Figure 4(a) shows the designed phase annular mask with zero padding, and the inset is the original mask with the annular thickness 43% of the pupil size. By using this mask, a new phase

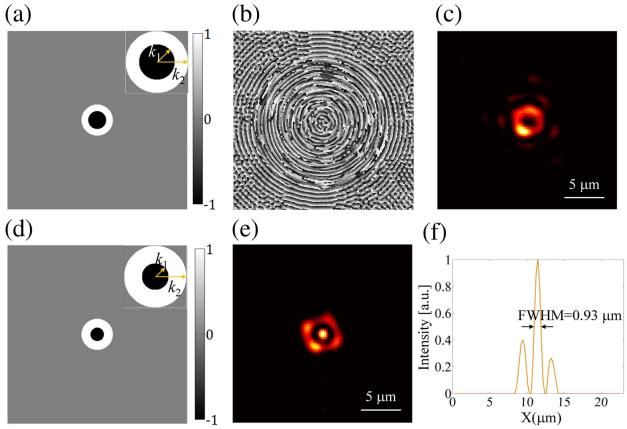


**Fig. 4.** Measurement results for creating structured light beams through the MMF by using phase annular masks. (a)–(c) Using a phase mask with the annular thickness 43% of pupil size; (d)–(f) using a phase mask with the annular thickness 64% of pupil size.

pattern can be obtained, as shown in Fig. 4(b). When the phase pattern is displayed on the SLM, a focal spot with a donut-like intensity distribution is created through the MMF and recorded using the CCD, as presented in Fig. 4(c). Due to the special property, the donut beams could be used for optical manipulation and fabrication [52,53]. Figure 4(d) gives a designed phase mask with the annular thickness 64% of the pupil size. The resulting focal spot is shown in Fig. 4(e). The FWHM of the focal spot is characterized with a value of 0.93 μm, as given in Fig. 4(f). We evaluate its PBR with a value to be approximately 250, obviously lower than that of the Gaussian focus, but this focal spot still stands over a background speckle. In fact, more complex circular symmetry masks could be applied in the Fourier domain, e.g., a super-oscillation mask, thus enabling the creation of a smaller focal spot [54].

We have demonstrated that as the Gaussian focus is coupled near the fiber core axis, the built filtering operator enables the creation of corresponding point spread functions through the MMF. Then, we investigate the excitation spot deviated from the fiber core axis by adjusting the microscope objective $MO_2$. As a Gaussian focus is coupled away from the fiber core axis with a distance of approximately 25 μm, the resulting off-axis hologram is recorded using the CMOS. The phase information of the speckle field is reconstructed from the recorded hologram. As the transformed phase pattern is displayed on the SLM and the object beam is blocked, the regenerated Gaussian focal spot is recorded using the CCD, as shown in Fig. 5(a). Figure 5(b) shows the same focal spot in Fig. 5(a) when the CCD exposure time is extended. It is shown that the position of the focal spot is deviated from the fiber core axis. By applying a phase mask with appropriate annular thickness in the virtual Fourier domain of the reconstructed speckle field (the selected spectrum), a new phase pattern could be obtained. As the phase pattern is displayed on the SLM, a focal spot with a donut-like intensity distribution is created, as presented in Fig. 5(c). Figure 5(d) gives the created donut beam recorded when the CCD exposure is extended. Thus, we prove that the proposed method could be exploited for the achievement of point spread function engineering deviated from the MMF core axis.

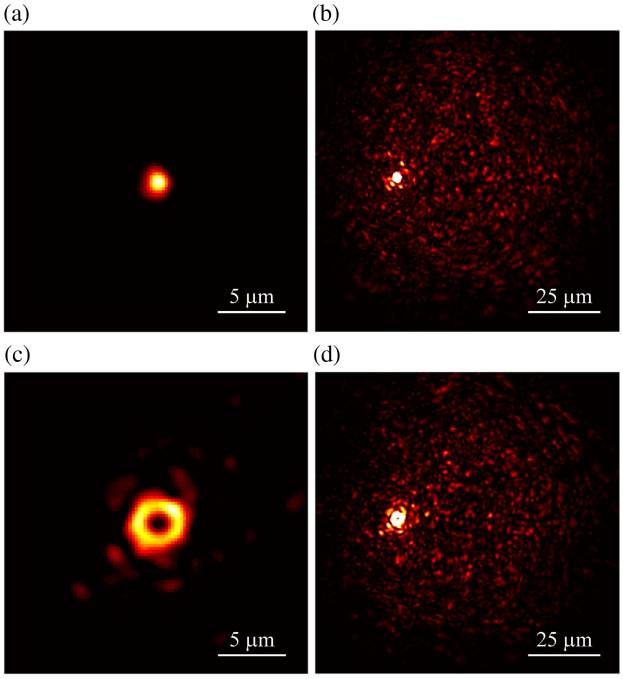


**Fig. 5.** Measurement results for the excitation spot deviated from the fiber core axis. (a) Regenerated Gaussian focal spot; (c) created donut beam; (b) and (d) the same focal spot in (a) and (c) when the CCD exposure time is extended, respectively.

## 4. CONCLUSION

In conclusion, we have demonstrated that DOPC could be developed for the achievement of modulating the reconstructed Gaussian focus, thus creating structured light beams. By applying circular symmetry masks in the virtual Fourier domain of the acquired scattered field, we realize the creation of two types of structured light beams via recording a single off-axis hologram. We first demonstrate the creation of a quasi-Bessel beam by using the amplitude annular filtering. The created quasi-Bessel beam shows a smaller size and longer depth of focus with respect to the regenerated Gaussian focus. We also apply the phase annular masks in the Fourier domain, thus creating a donut beam and smaller focal spot. In principle, arbitrary amplitude and/or phase circular symmetry masks could be applied in the Fourier domain, thus enabling the creation of the corresponding point spread functions. We expect that the proposed method might open up new opportunities for MMF-based super-resolution endoscopic microscopy as well as optical manipulation and fabrication through MMFs.

**Funding.** National Natural Science Foundation of China (11634010, 11774289, 61675170); Joint Fund of the National Natural Science Foundation of China and China Academy of Engineering Physics (U1730137); National Key R&D Program of China (2016YFA0300903, 2017YFA0303801); Beijing Graphene Innovation Program (Z181100004818003); National Equipment Program of China (ZDYZ2015-1).

**Disclosures.** The authors declare no conflicts of interest.

## REFERENCES

1. D. J. Richardson, J. M. Fini, and L. E. Nelson, "Space-division multiplexing in optical fibres," Nat. Photonics **7**, 354–362 (2013).
2. B. A. Flusberg, E. D. Cocker, W. Piyawattanametha, J. C. Jung, E. L. M. Cheung, and M. J. Schnitzer, "Fiber-optic fluorescence imaging," Nat. Methods **2**, 941–950 (2005).
3. G. Oh, E. Chung, and S. H. Yun, "Optical fibers for high-resolution *in vivo* microendoscopic fluorescence imaging," Opt. Fiber Technol. **19**, 760–771 (2013).
4. H. Yu, J. Park, K. Lee, J. Yoon, K. Kim, S. Lee, and Y. Park, "Recent advances in wavefront shaping techniques for biomedical applications," Curr. Appl. Phys. **15**, 632–641 (2015).
5. S. Rotter and S. Gigan, "Light fields in complex media: mesoscopic scattering meets wave control," Rev. Mod. Phys. **89**, 015005 (2017).
6. D. Bird and M. Gu, "Two-photon fluorescence endoscopy with a micro-optic scanning head," Opt. Lett. **28**, 1552–1554 (2003).
7. S. M. Popoff, G. Lerosey, R. Carminati, M. Fink, A. C. Boccara, and S. Gigan, "Measuring the transmission matrix in optics: an approach to the study and control of light propagation in disordered media," Phys. Rev. Lett. **104**, 100601 (2010).
8. A. Boniface, M. Mounaix, B. Blochet, R. Piestun, and S. Gigan, "Transmission-matrix-based point-spread-function engineering through a complex medium," Optica **4**, 54–59 (2017).
9. M. Vellekoop and A. P. Mosk, "Focusing coherent light through opaque strongly scattering media," Opt. Lett. **32**, 2309–2311 (2007).

10. O. Katz, E. Small, Y. Bromberg, and Y. Silberberg, "Focusing and compression of ultrashort pulses through scattering media," Nat. Photonics **5**, 372–377 (2011).
11. Z. Yaqoob, D. Psaltis, M. S. Feld, and C. Yang, "Optical phase conjugation for turbidity suppression in biological samples," Nat. Photonics **2**, 110–115 (2008).
12. X. Xu, H. Liu, and L. V. Wang, "Time-reversed ultrasonically encoded optical focusing into scattering media," Nat. Photonics **5**, 154 (2011).
13. M. Cui and C. Yang, "Implementation of a digital optical phase conjugation system and its application to study the robustness of turbidity suppression by phase conjugation," Opt. Express **18**, 3444–3455 (2010).
14. C. L. Hsieh, Y. Pu, R. Grange, G. Laporte, and D. Psaltis, "Imaging through turbid layers by scanning the phase conjugated second harmonic radiation from a nanoparticle," Opt. Express **18**, 20723–20731 (2010).
15. A. P. Mosk, A. Lagendijk, G. Lerosey, and M. Fink, "Controlling waves in space and time for imaging and focusing in complex media," Nat. Photonics **6**, 283–292 (2012).
16. Y. Choi, C. Yoon, M. Kim, T. D. Yang, C. Fang-Yen, R. R. Dasari, K. J. Lee, and W. Choi, "Scanner-free and wide-field endoscopic imaging by using a single multimode optical fiber," Phys. Rev. Lett. **109**, 203901 (2012).
17. T. Čižmár and K. Dholakia, "Exploiting multimode waveguides for pure fibre-based imaging," Nat. Commun. **3**, 1027 (2012).
18. W. Xiong, C. W. Hsu, Y. Bromberg, J. E. Antonio-Lopez, R. A. Correa, and H. Cao, "Complete polarization control in multimode fibers with polarization and mode coupling," Light Sci. Appl. **7**, 54 (2018).
19. B. Rahmani, D. Loterie, G. Konstantinou, D. Psaltis, and C. Moser, "Multimode optical fiber transmission with a deep learning network," Light Sci. Appl. **7**, 69 (2018).
20. S. Turtaev, I. T. Leite, T. Altwegg-Boussac, J. M. P. Pakan, N. L. Rochefort, and T. Čižmár, "High-fidelity multimode fibre-based endoscopy for deep brain in vivo imaging," Light Sci. Appl. **7**, 92 (2018).
21. S. Rothe, H. Radner, N. Koukourakis, and J. W. Czarske, "Transmission matrix measurement of multimode optical fibers by mode-selective excitation using one spatial light modulator," Appl. Sci. **9**, 195 (2019).
22. R. Di Leonardo and S. Bianchi, "Hologram transmission through multimode optical fibers," Opt. Express **19**, 247–254 (2011).
23. T. Čižmár and K. Dholakia, "Shaping the light transmission through a multimode optical fibre: complex transformation analysis and applications in biophotonics," Opt. Express **19**, 18871–18884 (2011).
24. H. Chen, Y. Geng, C. Xu, B. Zhuang, H. Ju, and L. Ren, "Efficient light focusing through an MMF based on two-step phase shifting and parallel phase compensating," Appl. Opt. **58**, 7552–7557 (2019).
25. I. N. Papadopoulos, S. Farahi, C. Moser, and D. Psaltis, "Focusing and scanning light through a multimode optical fiber using digital phase conjugation," Opt. Express **20**, 10583–10590 (2012).
26. D. Wang, E. H. Zhou, J. Brake, H. Ruan, M. Jang, and C. Yang, "Focusing through dynamic tissue with millisecond digital optical phase conjugation," Optica **2**, 728–735 (2015).
27. Y. Liu, C. Ma, Y. Shen, J. Shi, and L. V. Wang, "Focusing light inside dynamic scattering media with millisecond digital optical phase conjugation," Optica **4**, 280–288 (2017).
28. M. Jang, H. Ruan, H. Zhou, B. Judkewitz, and C. Yang, "Method for auto-alignment of digital optical phase conjugation systems based on digital propagation," Opt. Express **22**, 14054–14071 (2014).
29. K. Si, R. Fiolka, and M. Cui, "Fluorescence imaging beyond the ballistic regime by ultrasound-pulse-guided digital phase conjugation," Nat. Photonics **6**, 657–661 (2012).
30. R. Horstmeyer, H. Ruan, and C. Yang, "Guidestar-assisted wavefront-shaping methods for focusing light into biological tissue," Nat. Photonics **9**, 563–571 (2015).
31. M. Azimipour, F. Atry, and R. Pashaie, "Calibration of digital optical phase conjugation setups based on orthonormal rectangular polynomials," Appl. Opt. **55**, 2873–2880 (2016).
32. J. Yang, J. Li, S. He, and L. V. Wang, "Angular-spectrum modeling of focusing light inside scattering media by optical phase conjugation," Optica **6**, 250–256 (2019).
33. Y.-W. Yu, C.-C. Sun, X.-C. Liu, W.-H. Chen, S.-Y. Chen, Y.-H. Chen, C.-S. Ho, C.-C. Lin, T.-H. Yang, and P.-K. Hsieh, "Continuous amplified digital optical phase conjugator for focusing through thick, heavy scattering medium," OSA Continuum **2**, 703–714 (2019).
34. Z. Yu, M. Xia, H. Li, T. Zhong, F. Zhao, H. Deng, Z. Li, D. Li, D. Wang, and P. Lai, "Implementation of digital optical phase conjugation with embedded calibration and phase rectification," Sci. Rep. **9**, 1537 (2019).
35. N. Stasio, C. Moser, and D. Psaltis, "Calibration-free imaging through a multicore fiber using speckle scanning microscopy," Opt. Express **41**, 3078–3081 (2016).
36. R. Kuschmierz, E. Scharf, N. Koukourakis, and J. W. Czarske, "Self-calibration of lensless holographic endoscope using programmable guide stars," Opt. Lett. **43**, 2997–3000 (2018).
37. I. N. Papadopoulos, S. Farahi, C. Moser, and D. Psaltis, "High-resolution, lensless endoscope based on digital scanning through a multimode optical fiber," Biomed. Opt. Express **4**, 260–270 (2013).
38. R. Y. Gu, R. N. Mahalati, and J. M. Kahn, "Design of flexible multi-mode fiber endoscope," Opt. Express **23**, 26905–26918 (2015).
39. J. W. Czarske, D. Haufe, N. Koukourakis, and L. Büttner, "Transmission of independent signals through a multimode fiber using digital optical phase conjugation," Opt. Express **24**, 15128 (2016).
40. T. R. Hillman, T. Yamauchi, W. Choi, R. R. Dasari, M. S. Feld, Y. Park, and Z. Yaqoob, "Digital optical phase conjugation for delivering two-dimensional images through turbid media," Sci. Rep. **3**, 1909 (2013).
41. C. Ma, J. Di, Y. Zhang, P. Li, F. Xiao, K. Liu, X. Bai, and J. Zhao, "Reconstruction of structured laser beams through a multimode fiber based on digital optical phase conjugation," Opt. Lett. **43**, 3333–3336 (2018).
42. L. V. Amitonova, A. P. Mosk, and P. W. H. Pinkse, "The rotational memory effect of a multimode fiber," Opt. Express **23**, 20569–20575 (2015).
43. M. Plöschner, T. Tyc, and T. Čižmár, "Seeing through chaos in multimode fibres," Nat. Photonics **9**, 529–535 (2015).
44. D. E. B. Flaes, J. Stopka, S. Turtaev, J. F. de Boer, T. Tyc, and T. Čižmár, "Robustness of light-transport processes to bending deformations in graded-index multimode waveguides," Phys. Rev. Lett. **120**, 233901 (2018).
45. X. Zhu, A. Schülzgen, L. Li, and N. Peyghambarian, "Generation of controllable nondiffracting beams using multimode optical fibers," Appl. Phys. Lett. **94**, 201102 (2009).
46. W. A. Gambling, D. N. Payne, and H. Matsumura, "Mode conversion coefficients in optical fibers," Appl. Opt. **14**, 1538–1542 (1975).
47. H. Ma, H. Cheng, W. Zhang, L. Liu, and Y. Wang, "Generation of a hollow laser beam by a multimode fiber," Chin. Opt. Lett. **5**, 460–462 (2007).
48. C. Ma, J. Di, Y. Li, F. Xiao, J. Zhang, K. Liu, X. Bai, and J. Zhao, "Rotational scanning and multiple-spot focusing through a multimode fiber based on digital optical phase conjugation," Appl. Phys. Express **11**, 062501 (2018).
49. C. Ma, Y. Li, J. Zhang, P. Li, T. Xi, J. Di, and J. Zhao, "Lateral shearing common-path digital holographic microscopy based on a slightly trapezoid Sagnac interferometer," Opt. Express **25**, 13659–13667 (2017).
50. M. Mazilu, D. J. Stevenson, F. Gunn-Moore, and K. Dholakia, "Light beats the spread: non-diffracting beams," Laser Photon. Rev. **4**, 529–547 (2010).
51. L. Gao, L. Shao, C. D. Higgins, J. S. Poulton, M. Peifer, M. W. Davidson, X. Wu, B. Goldstein, and E. Betzig, "Noninvasive imaging beyond the diffraction limit of 3D dynamics in thickly fluorescent specimens," Cell **151**, 1370–1385 (2012).
52. T. Kuga, Y. Torii, N. Shiokawa, T. Hirano, Y. Shimizu, and H. Sasada, "Novel optical trap of atoms with a doughnut beam," Phys. Rev. Lett. **78**, 4713–4716 (1997).
53. M. Duocastella and C. B. Arnold, "Bessel and annular beams for materials processing," Laser Photon. Rev. **6**, 607–621 (2012).
54. A. M. H. Wong and G. V. Eleftheriades, "An optical super-microscope for far-field, real-time imaging beyond the diffraction limit," Sci. Rep. **3**, 1715 (2013).